Peroxide-doped apatites: Preparation and effect of synthesis parameters

N. Vandecandelaere, F. Bosc, C. Rey, C. Drouet *

CIRIMAT Carnot Institute — UMR CNRS/INPT/UPS 5085, University of Toulouse, Ensiacet, 4 allée Emile Monso, 31030 Toulouse cedex 4, France

Keywords:
Nanocrystalline apatite
Peroxide apatite
Synthesis parameters
Bioceramics
Hydroxyapatite
Bone infection

A B S T R A C T

This contribution focused on the *preparation* of peroxide-doped calcium phosphate apatites — in view of potential uses as bioactive bioceramics with antimicrobial functions, and on their *main physico-chemical characteristics*. Two synthesis routes were investigated. First, the hydrolysis of β-TCP in the presence of H_2O_2 was followed. However, only elevated concentrations in H_2O_2 in the medium or temperatures around 150 °C allowed us to reach the complete β-TCP-to-apatite hydrolysis process, and the obtained samples exhibited a high crystallinity state with no non-apatitic chemical environments. The second protocol tested consisted in the direct apatite precipitation in the presence of H_2O_2 in the medium (at room temperature). This protocol led to single-phased nanocrystalline apatites, and our data indicate that part of the apatitic OH^- ions were substituted by oxygenated species, and typically by peroxide ions (quantified). Physico-chemical modifications in the form of an improvement in crystallinity state, an increase in unit cell volume, and the presence of additional Raman bands were noticed and discussed.

1. Introduction

Calcium phosphates are major candidates for the design of bioceramic-based systems intended to bone regeneration (self-supported scaffolds, injectable bone cements, and implant coatings). In particular, calcium phosphate apatite compounds and predominantly nanocrystalline ones occupy a very peculiar position since they mimic the physico-chemical characteristics of bone mineral [1].

In addition to bare apatitic systems, a great deal of studies have also been devoted to explore associations between apatite crystals and a variety of (bio)molecules or drugs, such as antibiotics, anticancer drugs, growth factors, and vitamins [2], so as to convey additional properties to be exploited on a localized level at the site of implantation. Beside such hybrid organic/inorganic materials, it is however also possible to modify the biological and/or physico-chemical behavior of apatite systems by adequate ion substitutions. For example, the "doping" of calcium phosphate apatites by magnesium or strontium ions that has been reported (e.g. [3,4], either throughout the lattice or more specifically on the surface of the nanocrystals) is aimed at favoring osteoblast cell activity while limiting osteoclast resorptive functions, which may then be used for locally treating osteoporotic sites. The incorporation of silicate ions in phosphate crystallographic sites has also been shown to improve bone regeneration processes [5]. In another context, the substitution of calcium by lanthanide ions such as europium or terbium ions was also shown to convey luminescence properties to apatite particles that can then be exploited for other (not bone-related) applications such as cancer diagnosis [6–8].

The substitution of hydroxide OH^- ions (located in the so-called "apatitic channels" of the apatite lattice) by other anions has, in contrast, received globally less attention to this date, except for the particular case of A-type carbonation. The substitution of apatitic OH^- ions by oxygenated species, and especially by peroxide anions (i.e. species containing at least a O – O covalent bond), could however be seen as a way to modify apatite features that may find new applications in medicine, possibly for bone site asepsis after surgery. Indeed such oxygenated species are characterized by oxidizing properties that are naturally used in vivo (formation of Reactive Oxygenated Intermediates, ROI [9–11]) for fighting against infections. For instance, phagocytes locally produce superoxide (O_2^{2-}) ions to fight against bacteria [12,13]. The generation of ROI is also the mode of action of antibiotics such as fluoroquinolones [14]. This explains the use of peroxide-containing materials as antibacterial agents [13,15–17]. It should also be noted that natural pathways of elimination of such oxygenated species also exist in vivo, so as to regulate their overall activity. This regulation implies in particular specific enzymes such as superoxide dismutases and peroxydases (e.g. catalase), which ensure antioxidizing effects. Despite these statements, the development of oxygenated apatites as "reactive" implantable bioceramics has not received much development in medicine to date.

Although "oxygenated" apatites have not been overly investigated as compared to other substituted apatites, some past studies have however reported the possibility for apatitic channels to incorporate oxygenated species such as H_2O_2 or O_2 [18] or molecular ions including O_2^{2-} (the peroxide ion) and superoxide O_2^- [19]. Furthermore, the incorporation of such species in the apatite lattice was found to lead to specific modifications as compared to hydroxyapatite [18,20–22], and in particular a decrease in the FTIR intensity of OH^- bands and the appearance of additional Raman bands due to the presence of

* Corresponding author. Tel.: +33 5 34 32 34 11.
E-mail address: christophe.drouet@ensiacet.fr (C. Drouet).

http://dx.doi.org/10.1016/j.powtec.2013.09.015

peroxide O_2^{2-} ions (in particular at 750 cm^{-1} due to the symmetrical vibration of the O_2^{2-} ion). Unit cell parameters were also found to be altered upon apatite "oxygenation", although varying results were reported probably due to different synthesis protocols resulting in different oxygenated species and apatite compositions [18,20].

Taking into account the above statements, the present contribution aims at determining with further details the physico-chemistry of oxygenated apatites which could find future applications for example in bone infection treatments. In this original contribution, the preparation of peroxide-doped apatites was examined, and the impact of synthesis conditions on their physico-chemical characteristics – which we followed by several complementary techniques (XRD, FTIR, Raman, chemical analyses, and SEM) – was explored. Two different synthesis routes were considered in the presence of H_2O_2 in the reaction medium: 1) the hydrolysis of beta tricalcium phosphate (β-TCP) into apatite (a type of protocol initiated in early studies [18,23]), and 2) the direct apatite precipitation at room temperature from aqueous calcium and phosphate solutions.

2. Materials and methods

2.1. Preparation of peroxide-doped apatites

Two types of synthesis protocols were used in this work, either based on the hydrolysis of β-TCP (β-$Ca_3(PO_4)_2$) or on direct precipitation. In both cases, hydrogen peroxide/water media were used.

In the first case, 500 mg of β-TCP (previously synthesized from calcining amorphous tricalcium phosphate at 900 °C for 24 h [24]) was mixed with 30 mL of hydrogen peroxide H_2O_2 (stock solution at 110 vol. oxygen, equivalent to 9.82 mol/L H_2O_2) in deionized water in a closed container, and then heated to 100 °C for 24 h. After cooling, the compounds obtained for varying starting amounts of H_2O_2 were filtered on Büchner funnel and freeze-dried prior to analysis. Table 1 reports the concentrations in hydrogen peroxide that were tested in this work.

In the second protocol, direct precipitations were carried out in a way similar to the previously reported preparation of nanocrystalline biomimetic apatites [25] but in the presence of increasing amounts of H_2O_2 in the medium. A solution «A» containing 0.3 M of calcium nitrate ($Ca(NO_3)_2 \cdot 4H_2O$) was prepared in a mixture of H_2O_2/H_2O in variable proportions (see Table 2). A solution «B» of di-ammonium hydrogenphosphate ($(NH_4)_2HPO_4$, 0.6 M, was prepared in parallel in the same H_2O_2/H_2O medium. A volume of solution «A» was then poured into the doubled volume of solution «B», under stirring. The precipitation medium was then left to mature for 3 days at room temperature before filtration on Büchner funnel and freeze-drying.

2.2. Physico-chemical characterization

The nature and crystallographic structural features of the crystalline phases obtained in this work were investigated by X-ray diffraction (XRD) using a Seifert XRD 3000 TT diffractometer (Cu Kα1Kα2 radiation). The counting time was of 60 s for every step of 0.04°, typically in the 2θ range 20–70°. Unit cell parameters and volume were evaluated by XRD data treatment thanks to the JANA 2006 software, considering the systems as single-phased apatites ($P6_3/m$ space group).

Table 1
Initial proportions of H_2O_2 tested for the β-TCP synthesis route.

Sample reference	Vol.% of H_2O_2 stock solution (at 110 vol. oxygen) in the medium	Initial molar concentration in H_2O_2 in the medium (M)
H0%	0%	0
H5%	5%	0.49
H10%	10%	0.98
H25%	25%	2.46
H50%	50%	4.91
H75%	75%	7.37

Table 2
Initial proportions of H_2O_2 tested for the direct precipitation synthesis route.

Sample reference	Vol.% of H_2O_2 stock solution (at 110 vol. oxygen) in the medium	Molar concentration in H_2O_2 in the medium (M)
3d-10% H_2O_2	10%	0.98
3d-25% H_2O_2	25%	2.46
3d-50% H_2O_2	50%	4.91

Complementary analyses were run by Fourier transform infrared (FTIR) spectroscopy. Spectra were recorded on a Nicolet 5700 spectrometer in the range 400–4000 cm^{-1} (64 scans, resolution of 4 cm^{-1}). Spectral deconvolutions were carried out as previously described [25], after subtraction of a linear baseline, in the 400–800 cm^{-1} wavenumber range corresponding to the $\nu_2\nu_4(PO_4)$ and $\nu(OH)$ vibration modes of phosphate and hydroxide ions respectively, using the ORIGIN 8.1 software.

Raman spectra were recorded on a Horiba Jobin-Yvon LabRAM HR 800 spectrometer, typically in the range 100–4000 cm^{-1} using a $\lambda = 532$ nm laser. The acquisition was realized with an exposure time of 180 s and 6 accumulations for each point with an optical objective of ×100 and a diaphragm opening of 100 μm.

Scanning Electron Microscopy (SEM) analyses were performed on a LEO 435 VP microscope operated at 10–15 kV.

The chemical composition of the samples obtained was drawn from the measurement of ionic contents. The determination of the calcium and orthophosphate (PO_4^{3-} and HPO_4^{2-} ions) contents were obtained, after dissolution of the samples in perchloric acid, by way of EDTA complexometry and spectrophotometry (using the phospho–vanado–molybdenic complex, with $\lambda = 460$ nm) [26], respectively. Peroxide titration was performed by manganimetry titration using potassium permanganate $KMnO_4$ [27], exploiting the redox couple MnO_4^- (purple)/Mn^{2+} (colorless) and the reaction:

$$2MnO_4^- + 5H_2O_2 + 6H^+ \rightarrow 2Mn^{2+} + 5O_2 + 8H_2O. \quad (1)$$

For this titration, powder apatite samples were first dissolved in concentrated perchloric acid ($HClO_4$), and the obtained solution was then titrated by addition of a solution of $KMnO_4$ (0.005 M). The equivalence was then reached when the purple coloration of the permanganate ion persisted in the reacting medium.

3. Results and discussion

As mentioned above, two types of protocols were investigated in this work. The general goal was to obtain single-phased peroxide-doped apatites allowing varying amounts of peroxide doping. Also, the search for rather low crystallinity states and/or small constitutive crystals was an appealing secondary objective in view of obtaining potentially reactive apatite compounds [25] in view of future medical applications.

3.1. Synthesis by hydrolysis of β-TCP in H_2O_2/H_2O media

In a first step, we investigated the possible hydrolysis of β-TCP into apatite by heating in aqueous medium (mixtures of H_2O_2 and H_2O in pre-selected proportions), at a temperature of 100 °C for 24 h. Fig. 1 reports the XRD patterns obtained for 0, 25% and 75% (in volume) of H_2O_2 (stock solution at 110 vol. oxygen) in H_2O. In this figure, the characteristic patterns of the initial β-TCP compound (corresponding to JCPDS card No. 09-169) as well as of a reference stoichiometric hydroxyapatite HA (JCPDS card No. 09-432) were also added for comparative purposes.

Results indicated (see Fig. 1) that the sample treated at 100 °C for 24 h in the absence of H_2O_2 (sample H0%) was still composed of β-TCP, thus witnessing the absence of hydrolysis into apatite in these conditions. In contrast, increasing proportions of H_2O_2 in the reacting medium were found to allow a progression of the TCP-to-apatite

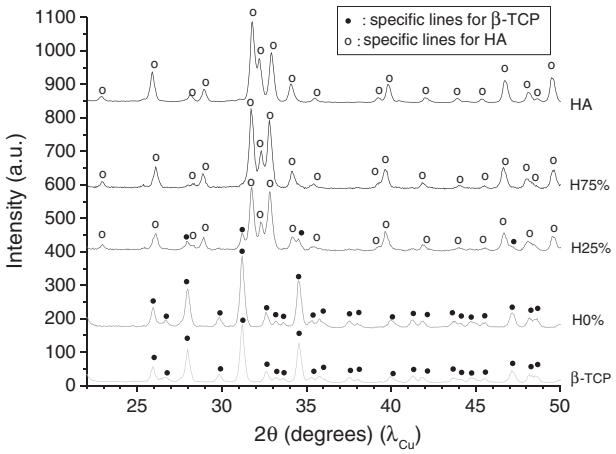

Fig. 1. XRD patterns for samples obtained by hydrolysis of β-TCP at 100 °C for increasing H_2O_2 proportions in the medium.

hydrolysis rate, as shown by the gradual decrease of the intensity of diffraction peaks related to β-TCP in favor of HA peaks. Among the conditions tested here however, only the sample H75% was found to be exclusively composed of an apatite phase, indicating that the complete hydrolysis of the β-TCP starting phase had then taken place. The introduction of hydrogen peroxide in the medium was thus found to favor this hydrolysis; this process being complete only for elevated proportions of H_2O_2 in the medium.

Besides, the XRD pattern of sample H75% (see Fig. 1) showed well-resolved diffraction peaks characteristic of a high degree of crystallinity for the apatite phase obtained by this hydrolysis route (contrarily to biomimetic nanocrystalline apatites [2,25]). SEM analysis carried out on the samples mentioned above (see the typical example of sample H75% in Fig. 2) showed that they were composed of acicular crystals of dimensions ranging from 0.5 to 2 μm in width and of several tens of microns in length. These micron-sized crystal dimensions (rather than nanometer-sized for bone apatite or synthetic analogs) agree well with the high degree of crystallinity noticed for all the samples, but are elements that disfavor surface reactivity aspects [25].

FTIR analysis was also carried out on sample H75%. Vibration bands characteristic of phosphate chemical environments in an apatite phase were observed at 471 cm^{-1} ($\nu_2(PO_4)$), 560/571/605 cm^{-1} ($\nu_4(PO_4)$), 960 cm^{-1} ($\nu_1(PO_4)$) and 1040/1089 cm^{-1} ($\nu_3(PO_4)$). Spectral deconvolution of the $\nu_2\nu_4(PO_4)$ region, in the 400–800 cm^{-1} range, was also processed as was explained previously in detail [25]. The absence of bands related to non-apatitic chemical environments for this sample was noted, which may probably be related to the mode of preparation (at 100 °C) which does not favor such hydrated environments [25]. The presence of a high proportion of hydrogen peroxide in the medium therefore did not have a detectable impact on the development of non-apatitic chemical environments on the constitutive apatite crystals. FTIR revealed, on the other hand, the presence of a non-negligible amount of apatitic HPO_4^{2-} ions (contribution at 550 cm^{-1}). The detection of an isolated band at 887 cm^{-1}, assignable to P–OH bonds in HPO_4^{2-} ions [1] also confirmed the presence of such species. These hydrogenphosphate ions are commonly observed in hydrolysis processes of different calcium phosphates (DCPD, DCPA, α-TCP) involving a dissolution–reprecipitation mechanism and an acidification of the solution related to the formation of apatite.

FTIR spectral analysis around 632 cm^{-1} (OH libration mode) only pointed out a very slight shoulder making it difficult at this stage to give direct evidence of the presence of regular apatitic OH^- ions. Taking into account the presence of peroxide ions in the medium, the low intensity of this libration mode is probably related to a high proportion of substitution of apatitic OH^- ions by peroxide ions (present in the medium) during the apatite formation. Bands due to peroxide ions are not, unfortunately, visualizable by the FTIR technique (being not suitable to detect symmetrical diatomic species such as O_2^{2-}, O_2^- or O_2) for direct confirmation; however the inset of Fig. 3 shows the appearance of additional contributive absorptions (as compared to the typical case of hydroxyapatite [25]) at 3524 and 3555 cm^{-1}. The location of these bands suggests a possible attribution to hydrogen bonds involving some "residual" OH^- ions in the lattice that could explain the slight libration shoulder at 632 cm^{-1}.

The above findings show that only elevated amounts of H_2O_2 in the medium (typically 75% in volume of stock solution at 110 vol. oxygen) allowed us to obtain a complete hydrolysis of β-TCP at 100 °C for 24 h. Generally speaking, the hydrolysis of β-TCP has been shown to follow a complex mechanism with several successive steps [18]: 1) the partial dissolution of the β-TCP phase, 2) the increase of Ca/P ratio in the reaction medium, 3) the formation of an apatite phase and 4) the evolution of this phase towards stoichiometry. However, these stages may be influenced by synthesis conditions such as temperature or duration of treatment. Additional experiments were then carried out (without H_2O_2) for up to 6 days at 100 °C or up to 48 h at 150 °C in view of obtaining single-phased apatite phases from β-TCP crystals. Some of the corresponding XRD patterns are reported in Fig. 4. Our results indicated that after 1, 2, 3 or 6 days of reaction at 100 °C, all samples remained composed of β-TCP (see for example samples H0% and H0c% corresponding to 1 and 6 days of reaction respectively). Therefore, an increase of reaction time (at 100 °C) did not allow for the TCP-to-apatite transformation. In contrast, the sample prepared by treatment of β-TCP at 150 °C for 48 h led to an XRD pattern corresponding to an apatite phase with no detectable traces of residual tricalcium phosphate (Fig. 4, pattern H0f). Therefore, in this work, an elevation of temperature was the only way to obtain the complete TCP-to-apatite transformation

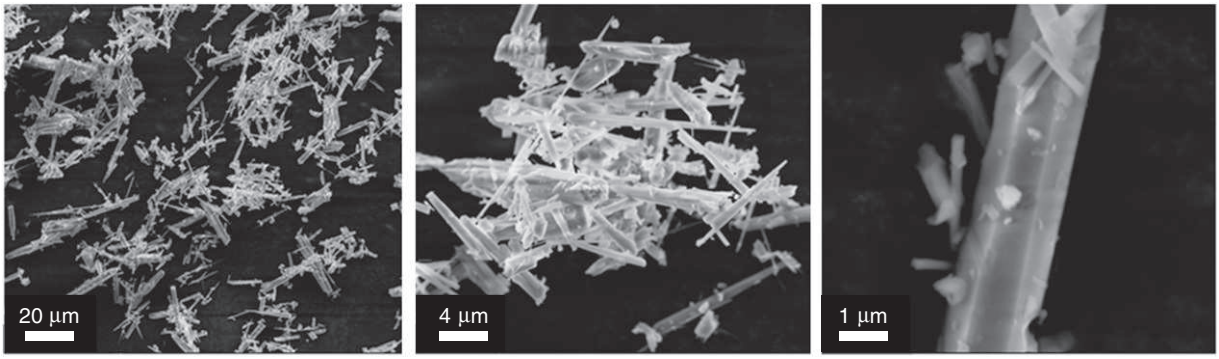

Fig. 2. SEM analysis of sample H75%.

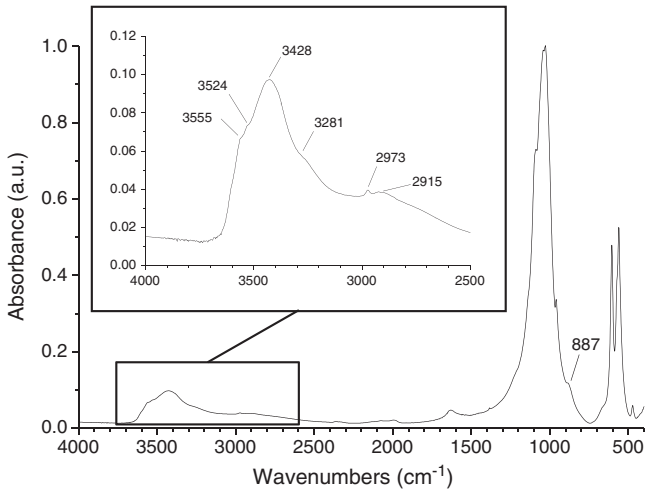

Fig. 3. FTIR spectrum for sample H75%.

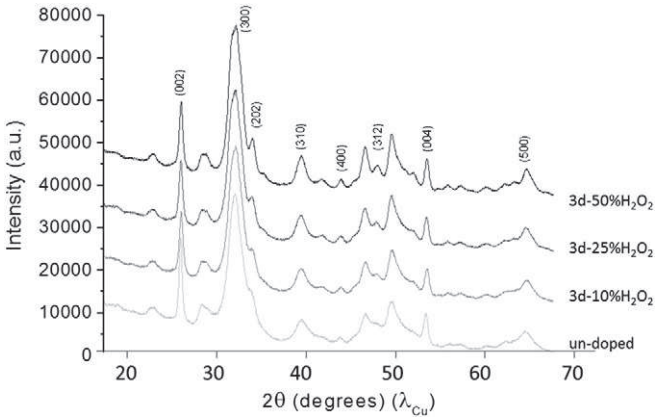

Fig. 5. XRD patterns for samples (3 days maturation) obtained by direct precipitation in varying proportions of H_2O_2.

in the absence of high amounts of H_2O_2 in the medium. Unfortunately, this XRD pattern is still indicative of a highly-crystallized state (with no non-apatitic ionic environment detectable by FTIR), which is thus bound to exhibit a low surface reactivity [25].

All our attempts to obtain, via this TCP hydrolysis process, low(er)-crystallinity apatite phases and/or containing non-apatitic features (as for bone apatite or biomimetic counterparts [1,28]) were unsuccessful. The investigation of this preparation route was thus discontinued and our attention turned to the exploration of a second type of protocol involving the direct precipitation, at room temperature, of (eventually peroxide-doped) apatite phases, which is described in the following section.

3.2. Synthesis by direct apatite precipitation in the presence of H_2O_2

This second protocol aimed at exploring the preparation of peroxide-doped apatites by direct precipitation from calcium and phosphate sources. Fig. 5 reports the XRD patterns obtained for samples matured for 3 days in a H_2O_2/H_2O medium corresponding to 0, 10%, 25% and 50% of H_2O_2 stock solution (110 vol. oxygen) in water. As can be seen, all the patterns obtained showed very similar features corresponding to poorly-crystallized apatite phases. No secondary phase could be detected. An increase in the overall resolution of the patterns was evidenced upon increasing the oxygen peroxide proportion in the medium, which is particularly visible for peaks (202) and (312). The presence of H_2O_2

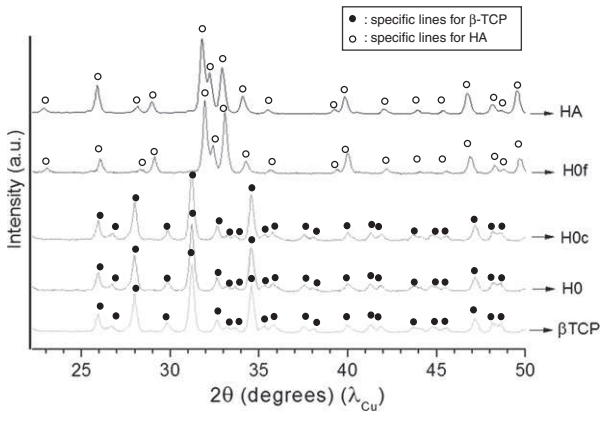

Fig. 4. XRD patterns for samples obtained by hydrolysis of β-TCP in varying conditions (H0 and H0c: 1 or 6 days of hydrolysis at 100 °C respectively; H0f: 2 days of hydrolysis at 150 °C).

in the precipitating medium thus tends to increase the crystallinity of the obtained apatite phase (for identical synthesis parameters); however the compounds obtained by this route remained poorly-crystallized.

XRD profile fitting analyses (JANA software) indicated that this crystallinity improvement was mainly linked to an increase of the mean crystallite width (determined from application to peak (310) of Hosemann and Vogel [29] or Scherrer formulas [30]), which continuously increased from 2.6 to 7.4 nm for H_2O_2 proportions in the medium from 0 to 50% (Table 3). In contrast, mean crystallite lengths remained essentially unchanged. The Hosemann and Vogel distortion parameter (giving a measure of the crystal disorder within the lattice) in the [002] direction, denoted g_{002}, was found to gradually decrease with the proportion of H_2O_2 in the medium: a drop of 15% was indeed observed for H_2O_2 proportion increasing from 10 to 50%. Although the value of g_{002} was systematically found to be greater for samples prepared in the presence of H_2O_2 rather than without H_2O_2, its decrease upon peroxidation of the medium could also contribute to the improvement in crystallinity observed.

The XRD profile analysis also pointed out a significant increase of the "a" unit cell parameter, from 9.432 to 9.470 Å, and a (moderate) decrease of the «c» parameter from 6.870 to 6.864 Å, when the initial amount of H_2O_2 increased from 0 to 50% (Table 3). This variation in unit cell parameters thus led to an increase of unit cell volume for syntheses realized in the presence of H_2O_2 (Table 3). The unit cell volume increased rapidly up to a concentration of H_2O_2 in solution of 2.46 M (corresponding to 25% stock solution of H_2O_2), and then stabilized at a value close to 533 $Å^3$ (Fig. 6). These findings strongly suggest the progressive incorporation of rather large chemical species in the apatitic core of the nanocrystals – most probably oxygenated species due to the presence of H_2O_2 – provoking a dilatation of the unit cell. Beyond an initial proportion of H_2O_2 in the medium around 25% of stock solution, the observed stabilization of the unit cell volume suggests however the attainment of a maximal amount of oxygenated species incorporated in the apatite core of the nanocrystals.

SEM observations of samples prepared in the presence or in the absence of H_2O_2 were then carried out (not shown); however no morphological differences were found.

In order to complete these analyses, a titration of incorporated peroxide groups was carried out by manganimetry assessments (see experimental section) for the samples 3d-10%H_2O_2, 3d-25%H_2O_2 and 3d-50%H_2O_2, leading to a peroxide content of 0.014 ± 0.001, 0.013 ± 0.001 and 0.018 ± 0.001 mmol/100 mg of apatite, respectively. These findings thus confirmed the presence of peroxide groups in the composition of these apatite samples. Note that this titration method only quantifies peroxide groups such as O_2^{2-} ions and possibly H_2O_2 molecules which could be associated, like water molecules, to these apatites. This titration method is not directly suited to quantify other (metastable) oxygenated species such as superoxide or ozonide ions.

Table 3
XRD profile fitting results (λCu) for nanocrystalline apatite synthesized at room temperature in various H_2O_2/H_2O media (3 days of maturation in solution).

Sample reference	Scherrer		Hosemann & Vogel	
	L(002) nm	L(310) nm	L(00l) nm	L(h00) nm
Un-doped	22.0 ± 0.1	3.8 ± 0.1	16.2 ± 0.1	2.6 ± 0.1
3d-10% H_2O_2	20.1 ± 0.2	7.6 ± 0.1	16.5 ± 0.3	5.7 ± 0.2
3d-25% H_2O_2	19.8 ± 0.1	8.3 ± 0.1	15.8 ± 0.1	6.4 ± 0.1
3d-50% H_2O_2	20.3 ± 0.3	9.3 ± 0.1	15.9 ± 0.6	7.4 ± 0.3
Sample reference	g_{002}	A-unit cell parameter Å	C-unit cell parameter Å	Unit cell volume Å^3
Un-doped	0.0071 ± 0.0001	9.432 ± 0.006	6.870 ± 0.002	529.3 ± 0.8
3d-10% H_2O_2	0.0100 ± 0.0004	9.464 ± 0.002	6.865 ± 0.001	532.5 ± 0.2
3d-25% H_2O_2	0.0095 ± 0.0003	9.469 ± 0.002	6.866 ± 0.002	533.1 ± 0.2
3d-50% H_2O_2	0.0085 ± 0.0020	9.470 ± 0.002	6.864 ± 0.001	533.1 ± 0.2

These radical ions are however unstable, their lifetime in solution is very short, and their decomposition may lead to peroxides that can then be titrated.

FTIR analyses were then carried out on these samples (Fig. 7). The spectra were all found to be characteristic of nanocrystalline biomimetic apatites, without additional bands. The OH^- bands at ca. 3570 and 631 cm^{-1} appeared less easily detectable for samples precipitated in the presence of hydrogen peroxide. This phenomenon could be related to the substitution of OH^- ions by oxygenated species such as peroxide ions (previously quantified) in the apatite lattice. Spectral deconvolution of the $\nu_2\nu_4(PO_4)$ region additionally unveiled a decrease of about 50% of the amount of non-apatitic HPO_4^{2-} ions (contribution at 530 cm^{-1}) in the presence of peroxide ions in the medium. These findings suggest that the maturation state of the apatite phase tends to improve in the presence of peroxides, which is thus accompanied by a decrease in non-apatite environments. The «accelerating» crystal growth effect mentioned above, as witnessed from XRD analyses by a noticeable increase in crystallinity state in the presence of hydrogen peroxide, is in good agreement with this result.

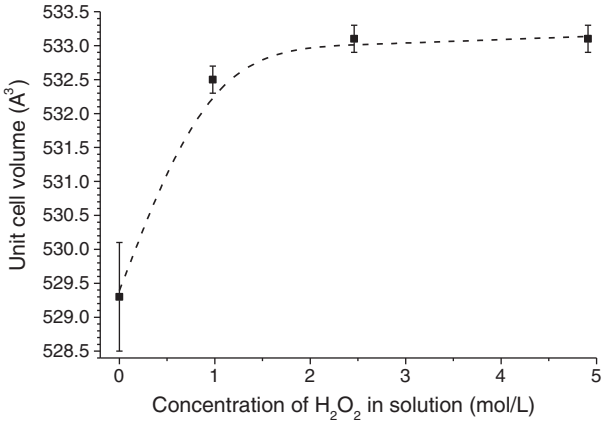

Fig. 6. Evolution of unit cell volume for samples prepared by direct precipitation versus initial concentration in H_2O_2 in the medium.

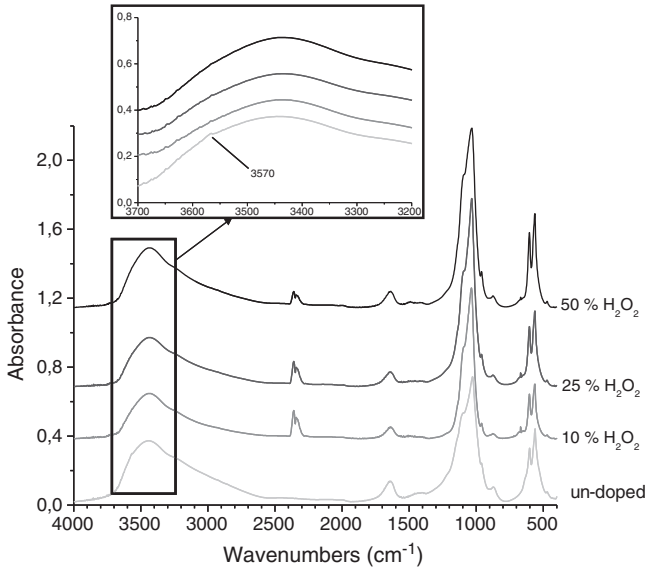

Fig. 7. FTIR spectra for samples (3 days maturation) obtained by direct precipitation in varying proportions of H_2O_2.

Raman spectroscopy analyses were carried out at this stage (Fig. 8). In addition to bands regularly observed for nanocrystalline apatites, the presence of additional Raman bands was evidenced for samples prepared in the presence of H_2O_2, in the form of 3 main modifications:

- m_1 in the range 750–850 cm^{-1}, constituted by 3 bands at 793, 827 and 845 cm^{-1}
- m_2 in the range 1080–1140 cm^{-1}, constituted by 4 bands at 1096, 1103, 1114 and 1124 cm^{-1}
- and m_3 in the range 2800–3100 cm^{-1}, constituted by 3 bands at 2858, 2883 and 2940 cm^{-1}.

Very few data are available in the literature on the Raman characteristics of peroxidized or oxygenated apatites. Rey [18] indicated that several types of peroxide ions could be found in apatite channels, such as «simple» peroxide ion O_2^{2-}, superoxide ion O_2^-, the more complex

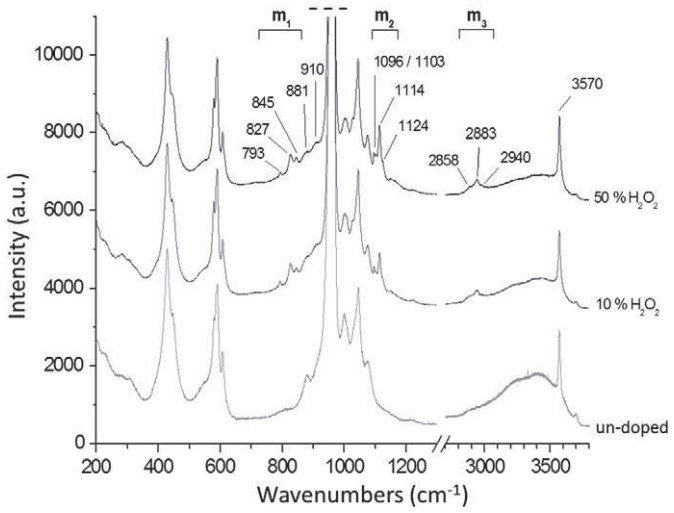

Fig. 8. Raman spectra for samples (3 days maturation) obtained by direct precipitation in varying proportions of H_2O_2 (the band at 960 cm^{-1} was truncated for greater visibility).

polyoxide species O_3^{2-} and O_4^{2-} ions, and molecular oxygen O_2 or hydrogen peroxide H_2O_2, and the following Raman band attributions were proposed:

- a band at 450 cm^{-1} attributed to large molecular species like O_3^{2-} ou O_4^{2-}
- a large asymmetrical group around 800 cm^{-1} attributed to the O – O vibration of different oxygenated species, including peroxide group
- a thin band at 1150 cm^{-1} attributed to superoxide O_2^-
- an intense band at 1552 cm^{-1} attributed to molecular oxygen O_2 formed by the decomposition of other metastable oxygenated species.

In the present study (Fig. 8), the presence of bands located at 450 cm^{-1} (relative to large molecular species) or at 1552 cm^{-1} (O_2) was not detected, suggesting that these chemical species are not present in detectable amounts in the prepared samples. In contrast, the m_1 bands observed between 750 and 850 cm^{-1} probably correspond to peroxide bands reported previously by Rey [18] around 800 cm^{-1} and globally assigned to a "O – O stretching" and by Zhao et al. [22] at 750 cm^{-1} assigned to the peroxide ion O_2^{2-}.

Moreover, bands from the m_2 region in the range 1080–1140 cm^{-1} can probably be related to the band observed at 1150 cm^{-1} by Rey [18] which was attributed to the vibration of the superoxide ion O_2^-. The yellowish color of samples obtained in the presence of H_2O_2 (in comparison to the white color of samples prepared without H_2O_2) is indeed an element in favor of the presence of at least traces of superoxide ion in our samples. The m_3 bands (between 2800 and 3100 cm^{-1}), on the other hand, do not seem to be easily assignable to bands previously described in the literature to our knowledge and their exact attribution remains at this point uncertain. Although this vibration domain could correspond to C – H stretching, the presence of organic compounds associated to the powders remains quite unlikely as no such species were involved in the synthesis.

Although bands related to OH^- ions in apatitic environment were not clearly visible by FTIR, the band at 3570 cm^{-1} is identifiable by Raman spectroscopy for all samples (doped and non-doped), thus revealing the presence of remaining OH^- ions in the lattice for all samples.

In addition, it can be noted that two low-intensity Raman bands at 881 and 910 cm^{-1} – also detectable for non-doped samples – were found to become more clearly visible for samples prepared in the presence of H_2O_2. A vibrational contribution in this range (e.g. 880 cm^{-1}) was attributed to HPO_4^{2-} ions in apatites [31]. This increase in intensity could probably be related to the improved crystallinity state of samples prepared in the presence of hydrogen peroxide, as was shown above by XRD analyses, thus allowing for better spectral resolution.

The above findings thus indicate that it is possible, by way of direct precipitation, to synthesize peroxide-loaded nanocrystalline apatites in the presence of hydrogen peroxide in the precipitating medium, without formation of detectable secondary phases (even for high H_2O_2 contents, tested here up to 50% of stock solution at 110 vol. oxygen). The presence of H_2O_2 in the precipitating medium led to various physico-chemical modifications: the crystallinity state of the apatite phase was found to improve for increasing H_2O_2 proportions in the medium; a noticeable increase in unit cell volume was evidenced strongly supporting the idea of an incorporation of oxygenated species in the apatite lattice; peroxide ions were in particular evidenced and quantifiable by manganimetry, showing that this synthesis route was appropriate to prepare apatite samples with varying peroxide contents; the presence of at least traces of superoxide ion was also suspected; and the presence of additional Raman bands linked to such oxygenated species was pointed out. Based on these elements, associated to the nano-sized dimensions of the constitutive crystals and to the remaining presence of non-apatitic species, this synthetic route appears as very appropriate for the production of peroxide-doped reactive apatite materials.

4. Concluding remarks

In this contribution, two ways of preparation of peroxide-doped calcium phosphate apatites were investigated.

First, the hydrolysis of β-TCP in the presence of H_2O_2 was followed. By this protocol, however, only elevated concentrations in H_2O_2 in the medium allowed us to obtain single-phased apatite compounds (attesting for the complete TCP-to-apatite hydrolysis) at 100 °C, unless higher temperatures (tested here: 150 °C) were used. Moreover, the apatite samples obtained by this route always exhibited a high crystallinity state with no non-apatitic chemical environments (the presence of which has been related to the surface reactivity of apatitic compounds [1–3,32]).

The second protocol tested consisted in the direct apatite precipitation from an aqueous calcium and phosphate solutions and in the presence of H_2O_2 in the medium (at room temperature). This route allowed us to obtain single-phased nanocrystalline apatites in a wide range of H_2O_2 proportions in the precipitating medium. Moreover, our data indicate that part of the apatitic OH^- ions were replaced in this case by oxygenated species, and typically by peroxide ions (quantified) and at least traces of superoxide ions. Several physico-chemical modifications such as an improvement in crystallinity state, an increase in unit cell volume, and the presence of additional bands in the Raman spectra were noticed and discussed.

Acknowledgments

This work was financially supported by the French "Agence Nationale de la Recherche" (ANR) by way of the PICF *BioCapabili* project.

References

[1] D. Eichert, C. Drouet, H. Sfihi, C. Rey, C. Combes, Nanocrystalline apatite-based biomaterials: synthesis, processing and characterization, in: J.B. Kendall (Ed.), Biomaterials Research Advances, Nova Science Publishers, 2007, pp. 93–143.
[2] J. Gomez-Morales, M. Iafisco, J. Manuel Delgado-Lopez, S. Sarda, C. Drouet, Progress on the preparation of nanocrystalline apatites and surface characterization: overview of fundamental and applied aspects, Prog. Cryst. Growth Charact. Mater. 59 (2013) 1–46.
[3] C. Drouet, M. Carayon, C. Combes, C. Rey, Surface enrichment of biomimetic apatites with biologically-active ions Mg2+ and Sr2+: a preamble to the activation of bone repair materials, Mater. Sci. Eng. C 28 (2008) 1544–1550.
[4] J. Christoffersen, M.R. Christoffersen, N. Kolthoff, O. Barenholdt, Effects of strontium ions on growth and dissolution of hydroxyapatite and on bone mineral detection, Bone 20 (1997) 47–54.
[5] A.E. Porter, N. Patel, J.N. Skepper, S.M. Best, W. Bonfield, Effect of sintered silicate-substituted hydroxyapatite on remodelling processes at the bone–implant interface, Biomaterials 25 (2004) 3303–3314.
[6] A. Al-Kattan, F. Errassifi, A. Sautereau, S. Sarda, P. Dufour, A. Barroug, I. Dos Santos, C. Combes, D. Grossin, C. Rey, C. Drouet, Medical potentialities of biomimetic apatites through adsorption, ionic substitution, and mineral/organic associations: three illustrative examples, Adv. Eng. Mater. 12 (2010) B224–B233.
[7] A. Al-Kattan, P. Dufour, J. Dexpert-Ghys, C. Drouet, Preparation and physicochemical characteristics of luminescent apatite-based colloids, J. Phys. Chem. C 114 (2010) 2918–2924.
[8] A. Al-Kattan, S. Girod-Fullana, C. Charvillat, H. Ternet-Fontebasso, P. Dufour, J. Dexpert-Ghys, V. Santran, J. Bordere, B. Pipy, J. Bernad, C. Drouet, Biomimetic nanocrystalline apatites: emerging perspectives in cancer diagnosis and treatment, Int. J. Pharm. 423 (2012) 26–36.
[9] V.I. Lushchak, Oxidative stress and mechanisms of protection against it in bacteria, Biochem.-Moscow 66 (2001) 476–489.
[10] S.B. Farr, T. Kogoma, Oxidative stress responses in *Escherichia coli* and *Salmonella typhimurium*, Microbiol. Rev. 55 (1991) 561–585.
[11] G. Storz, L.A. Tartaglia, S.B. Farr, B.N. Ames, Bacterial defenses against oxidative stress, Trends Genet. 6 (1990) 363–368.
[12] B. Rada, T.L. Leto, Oxidative innate immune defenses by Nox/Duox family NADPH oxidases, Contrib. Microbiol. 15 (2008) 164–187.
[13] J.L. Shenep, D.C. Stokes, W.T. Hughes, Lack of antibacterial activity after intravenous hydrogen peroxide infusion in experimental *Escherichia coli* sepsis, Infect. Immun. 48 (1985) 607–610.
[14] I. Albesa, M.C. Becerra, P.C. Battan, P.L. Paez, Oxidative stress involved in the antibacterial action of different antibiotics, Biochem. Biophys. Res. Commun. 317 (2004) 605–609.

[15] O. Feuerstein, D. Moreinos, D. Steinberg, Synergic antibacterial effect between visible light and hydrogen peroxide on *Streptococcus mutans*, J. Antimicrob. Chemother. 57 (2006) 872–876.
[16] J. Muller, S. Janz, Modulation of the H_2O_2-induced SOS response in *Escherichia coli* PQ300 by amino-acids, metal chelators, antioxidants and scavengers of reactive oxygen species, Environ. Mol. Mutagen. 22 (1993) 157–163.
[17] R. Pedahzur, O. Lev, B. Fattal, H.I. Shuval, The interaction of silver ions and hydrogen peroxide in the activation of *Escherichia coli* — a preliminary evaluation on a new long-acting residual drinking water disinfectant, Water Sci. Technol. 31 (1995) 123–129.
[18] C. Rey, Étude des Relations Entre Apatites et Composés Moléculaires Oxygénés, (PhD thesis) INP Toulouse, France, 1984.
[19] J. Dugas, C. Rey, Electron-spin resonance characterization of superoxide ions in some oxygenated apatites, J. Phys. Chem. 81 (1977) 1417–1419.
[20] J.-C. Trombe, Mise en Evidence d'une Peroxyapatite Phosphocalcique, C. R. Acad. Sci. Paris 273 (1971) 972–974.
[21] H.G. Yu, H.L. Zhang, X.M. Wang, Z.W. Gu, X.D. Li, F. Deng, Local structure of hydroxy–peroxy apatite: a combined XRD, FT-IR, Raman, SEM, and solid-state NMR study, J. Phys. Chem. Solids 68 (2007) 1863–1871.
[22] H.C. Zhao, X.D. Li, J.X. Wang, S.X. Qu, J. Weng, X.D. Zhang, Characterization of peroxide ions in hydroxyapatite lattice, J. Biomed. Mater. Res. 52 (2000) 157–163.
[23] D.R. Simpson, Oxygen rich apatite, Am. Mineral. 54 (1969) 560.
[24] C. Rey, C. Combes, C. Drouet, S. Somrani, Tricalcium phosphate-based ceramics, in: T. Kokubo (Ed.), Bioceramics and Their Clinical Applications, Woodhead Publishing Limited, Cambridge, England, ISBN: 978 1 84569 204 9, 2008, pp. 326–366.
[25] N. Vandecandelaere, C. Rey, C. Drouet, Biomimetic apatite-based biomaterials: on the critical impact of synthesis and post-synthesis parameters, J. Mater. Sci. Mater. Med. 23 (2012) 2593–2606.
[26] G. Charlot, Chimie Analytique Quantitative, Masson, Paris, 1974.
[27] G. Charlot, Les méthodes de la chimie analytique: Analyse Qualitative et minérale, Masson, Paris, 1966.
[28] C. Rey, C. Combes, C. Drouet, M. Glimcher, Bone mineral: update on chemical composition and structure, 3rd Meeting on Bone, Quality, 2009. 1013–1021.
[29] W. Vogel, R. Hosemann, Evaluation of paracrystalline distortions from line broadening, Acta Crystallogr. A 26 (1970) 272–277.
[30] P. Scherrer, P. Scherrer, Estimation of size and internal structure of colloidal particles by means of Röntgen rays, Gott. Nachr. 2 (1918) 98–100.
[31] G. Penel, G. Leroy, C. Rey, E. Bres, MicroRaman spectral study of the PO_4 and CO_3 vibrational modes in synthetic and biological apatites, Calcif. Tissue Int. 63 (1998) 475–481.
[32] C. Rey, C. Combes, C. Drouet, H. Sfihi, A. Barroug, Physico-chemical properties of nanocrystalline apatites: implications for biominerals and biomaterials, Mater. Sci. Eng. C 27 (2007) 198–205.